Formation Control of Mobile Robots with Active Obstacle Avoidance

LIU Shi-Cai[1, 2] TAN Da-Long[1] LIU Guang-Jun[3]

Abstract In this paper, the formation control and obstacle avoidance problems are dealt with a unified control algorithm, which allows the follower to avoid obstacle while maintaining desired relative bearing or relative distance from the leader. In the known leader-follower robot formation control literature, absolute motion states of the leader robot are required to control the followers, which may not be available in some environments. In this research, the leader-follower robot formation is modelled and controlled in terms of the relative motion states between the leader and follower robots. The absolute motion states of the leader robot are not required in the proposed formation controller. Furthermore, the research has been extended to a novel obstacle avoidance scheme based on sensing the relative motion between robot and obstacle. Experimental investigation has been conducted using the platform consisted of three nonholonomic mobile robots and computer vision system, and the results have demonstrated the effectiveness of the proposed methods.

Key words Formation control, obstacle avoidance, relative motion states

1 Introduction

Various control strategies for mobile robot formation have been reported in the literature, including the leader-follower schemes[1∼3], behavior-based methods[4∼6], and virtual structure techniques[7]. Among them, the leader-follower approach has been well recognized and become the most popular approach: one or more robots are selected as leaders and are responsible for guiding the formation. The rest of robots are required to follow the leader with some prescribed offsets. The problem of modeling and control of leader-follower formation has been studied by many researchers[1∼3]. More recently, Vidal *et al.*[8] proposed a formation control approach using the optical flows.

To the best of the authors' knowledge, all the known leader-follower control methods directly or indirectly rely on the absolute motion states in a global frame. However, the global motion states may not be available in some environments as there are no suitable global motion sensors. In this research, the control of follower robots is based on the relative motion states, in view of the followers, between robots or robot and obstacles. It eliminates the need of measurement or estimation of the absolute velocity and angular velocity of leader and enables formation control using vision systems carried by the follower robots. The proposed formation controller also does not require other media, such as the optical flows in [8].

Another challenge for formation control is active obstacle avoidance for the follower robots. This problem has been barely studied in the literature. In the leader-follower formation control approach, if the leader robot can detect obstacles, it can use the existing algorithm to navigate itself, while other robots can passively follow the leader. However, if a follower robot encounters an obstacle, in many situations it cannot navigate itself, because the follower robot needs not only to perform obstacle avoidance but also formation recovering after it passes around obstacles. For these reasons, an effective approach is to let the leader robot influence the obstacle avoidance behavior for the follower robot and guide it to a free area around the leader robot. Otherwise, the follower robot may again encounter the obstacle that it has just avoided.

Based on the above considerations, a novel obstacle avoidance control scheme is developed using a derived relative kinematics model. The proposed approach allows the follower robot to avoid obstacle while keeping a desired bearing or distance from the leader. Since the formation is partially kept when the follower robot is moving around an obstacle, cooperation between the two robots will not be completely interrupted by the obstacle.

2 Formation control

2.1 Formulation of the nonholonomic mobile robot system

As indicated in Fig. 1(a), the mobile robots are car-like platforms. The kinematics equations of the robots are given by the equations of the form

$$\begin{pmatrix} \dot{x}_{ci} \\ \dot{y}_{ci} \end{pmatrix} = \begin{pmatrix} \cos\phi_i & -d\sin\phi_i \\ \sin\phi_i & d\cos\phi_i \end{pmatrix} \begin{pmatrix} v_i \\ \omega_i \end{pmatrix} \tag{1}$$

$$\dot{\phi}_i = \omega_i$$

where $(x_{ci} \quad y_{ci})^{\mathrm{T}}$ are the coordinates of the center of mass P_c in the world coordinates system, and ϕ_i is the heading angle of the robot. v_i and ω_i are the linear and angular velocities of the robot R_i, respectively. d is the distance from point P_c to the center of the wheel axis P_o.

Set $u = (v_i \quad \omega_i)^{\mathrm{T}}$ as the state variable. The dynamic equation of the robot R_i in the local coordinates system is given by

$$\overline{H}\dot{u}_i + \overline{V}u_i = \overline{B}\tau_i \tag{2}$$

where

$$\overline{H} = \begin{pmatrix} m + 2I_w/r^2 & \\ & I + (m_c - 2m_w)d^2 + 2b^2 I_w/r^2 \end{pmatrix}$$

$$\overline{V} = \begin{pmatrix} & -(m - 2m_w)d\dot{\phi}_i \\ (m - 2m_w)d\dot{\phi}_i & \end{pmatrix}$$

$$\overline{B} = \begin{pmatrix} 1/r & 1/r \\ b/r & -b/r \end{pmatrix} \quad and \quad \tau_i = (\tau_r \quad \tau_l)^{\mathrm{T}}$$

for $m = m_c + 2m_w$ and $I = I_c + 2m_w(b^2 + d^2) + 2I_m$. m_c and m_w are the mass of the robot without two driving wheels and the mass of each driving wheel, respectively. I_c is the moment of inertia of the platform without the driving wheels about a vertical axis through P_c. I_m and I_w are the

Received January 3, 2006; in revised form July 29, 2006
Supported in part by National High Technology Research and Development Program of P. R. China (2001AA422140)
1. Robotics Laboratory, Shenyang Institute of Automation, Chinese Academy of Sciences, Shenyang 110016, P. R. China 2. Graduate University of the Chinese Academy of Sciences, Beijing 100049, P. R. China 3. Department of Aerospace Engineering, Ryerson University, Toronto M5B 2K3, Canada
DOI: 10.1360/aas-007-0529

moment of inertia of each wheels about the wheel axis and a wheel diameter, respectively. r is the radius of each driving wheel, and b is the distance between each driving wheel and the symmetry axis. τ_r and τ_l are the torques generated by the right and left motors, respectively. It is easy to prove that the following property holds

$$u_i^{\mathrm{T}}(\dot{\bar{H}} - 2\bar{(V)})u_i = 0$$

which will be used to prove the stability of the robot control system.

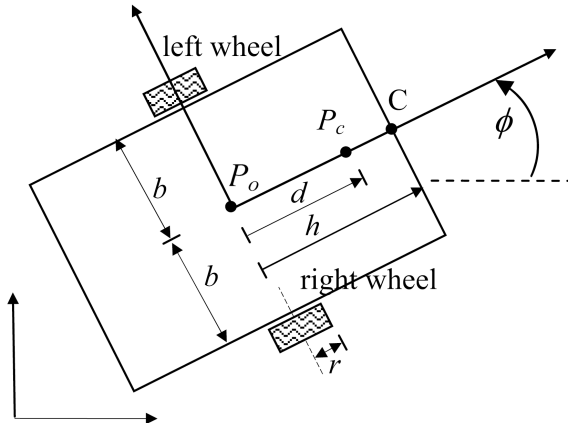

(a) Notation for the geometry of the nonholonomic mobile robot

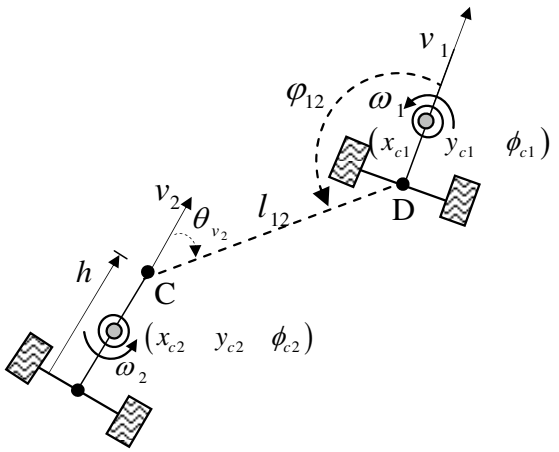

(b) Two robots formation using leader-follower controller

Fig. 1 Mobile robots formation

2.2 Formulation of the leader-follower robots system

As shown in Fig. 1(b), the follower robot R_2 follows the leader robot R_1. The vision-based relative motion sensor is mounted at the reference point C on the follower robot R_2. The goal of the formation control is that robot R_2 tracks R_1 with a desired distance l_{12}^d and a desired relative bearing φ_{12}^d between the two robots. As shown in Fig. 1 (b), the distance between the reference points of the two robots is denoted by l_{12} and the relative bearing between the two robots is denoted by φ_{12}. The angle between velocity $\boldsymbol{v}_2$ and line $\boldsymbol{l}_{12}$ is given by θ_{v2}, and $\theta_{v2} = \pi - \varphi_{12} - \theta_{12}$. The parameter h is the distance from the point Po to the reference point C.

Denote $q = (l_{12} \quad \varphi_{12})^{\mathrm{T}}$ as the state variable, and $u_2 = (v_2 \quad \omega_2)$ as the input of the robot formation system. Based on the work [1∼3], the leader-follower robots formation system can be described by

$$\dot{q} = L(q \quad v_1 \quad \omega_1) + F(q)u_2 \tag{3}$$

$$\dot{\phi}_{12} = \omega_1 - \omega_2$$

where

$$L = \begin{pmatrix} -v_1\cos\varphi_{12} \\ v_1\sin\varphi_{12}/l_{12} - \omega_2 \end{pmatrix}$$

and

$$F = \begin{pmatrix} -\cos\theta_{v2} & h\sin\theta_{v2} \\ -\sin\theta_{v2}/l_{12} & h\cos\theta_{v2}/l_{12} \end{pmatrix}$$

The terms L and F present the influence introduced by the motions of the leader and the follower, respectively.

Taking the measurement errors introduced by the latency and the noise of the visual sensor into account, the system can be presented as

$$\dot{q} = [L(q \quad \widehat{v}_1 \quad \widehat{\omega}_1) + F(q)\widehat{u}_2] + F(q)(u_2 - \widehat{u}_2) + \Delta_s \tag{4}$$

where the term $M_R(q) = [L(q \quad \widehat{v}_1 \quad \widehat{\omega}_1) + F(q)\widehat{u}_2]$ can be described in term of the relative motion states between two robots, *i.e.*,

$$M_R = \begin{pmatrix} v_R\cos\theta_{vR} \\ v_R\sin\theta_{vR}/l_{12} - \omega_R \end{pmatrix} \tag{5}$$

where v_R and ω_R are the linear and angular velocities, respectively, from the view of the visual sensor fixed on the follower robot, by which the leader robot is relative to the follower robot. θ_{vR} is the bearing from the vector v_R to the line $\boldsymbol{l}_{12}$. It should be noted that the measured relative velocity v_R contains not only the effect of relative linear velocity between the two robots but also the effect of the angular velocity of the follower robot. The vector $\widehat{u}_2$ is the corresponding velocity of the follower robot when v_R and ω_R are measured, and Δ_s is the part of the uncertainty introduced by the latency and the noise of the visual sensor. In the following sections, Δ_s is assumed to be zero to simplify the analysis and the design of the formation control system. The following property holds on for the robot formation

$$\gamma_1 h \geq l_{12} \geq \gamma_2 h \tag{6}$$

due to the limitations of the robot geometry and the visual field of the motion sensor. γ_1 and γ_2 are positive constants.

The internal dynamics[9] of the leader-follower robot formation system is given by

$$\dot{\phi}_{12} = -A_\theta \sin(\phi_{12} - \alpha_0) + \omega_1 + \Gamma(q \quad \dot{q}) \tag{7}$$

where $A_\theta = \sqrt{(k_a)^2 + (k_b)^2}$, $\alpha_0 = \arctan(k_b/k_a)$, and $\Gamma(q \quad \dot{q}) = [-\sin\theta_{v2} \quad l_{12}\cos\theta_{v2}]\dot{q}/h$ for $k_a = (v_1 - \omega_1 l_{12}\sin\varphi_{12})/h$ and $k_b = \omega_1 l_{12}\cos\varphi_{12}/h$, respectively. The zero dynamics[9] of the formation system is given by

$$\dot{\phi}_{12} = -A_{\theta_0}\sin(\phi_{12} - \alpha_0) + \omega_1 \tag{8}$$

where A_{θ_0} is the corresponding value of A_θ for $q = q_d$ and $\dot{q} = 0$. Thus, the zero dynamics (8) is stable under the assumption $A_{\theta_0} \geq \omega_1$.

2.3 Control of leader-follower robots system backstepping kinematics into dynamics

In this subsection, a leader-follower formation controller is designed to make the follower robot track the leader robot with a given formation configuration. The controller is developed by combining a kinematics-based formation tracking controller and a dynamics-based velocity tracking controller. The combination is conducted using backstepping, and the asymptotic stability is guaranteed by Lyapunov theory. Moreover, this control algorithm can stabilize the whole leader-follower robot formation system in the presence of velocity tracking error of the dynamics system.

Set $u_{2d} = \bar{u}_{2d} + \tilde{u}_{2d}$ as the formation controller and $\tilde{u}_2 = u_2 - u_{2d}$ as the velocity tracking error of the robot dynamics; system (4) can be presented as

$$\dot{q} = M_R + F(q)(\bar{u}_{2d} + \tilde{u}_{2d} - \widehat{u}_2 + \tilde{u}_2) \tag{9}$$

The kinematics-based formation controller is designed as

$$u_{2d} = \widehat{u}_2 - F^{-1}(M_R + K_q(q - q_d)) \tag{10}$$

where $K_q = \mathrm{diag}(k_{q_1} \quad k_{q_2})$ and k_{q_1} and k_{q_2} are positive constants, and $q_d = (l_{12}^d \quad \varphi_{12}^d)^{\mathrm{T}}$ is the desired configuration for the robot formation. Furthermore, $\bar{u}_{2d}$ and $\tilde{u}_{2d}$ in (9) are designed as $\bar{u}_{2d} = \widehat{u}_2$ and $\tilde{u}_{2d} = -F^{-1}(M_R + K_q(q - q_d))$, respectively.

By applying the feedback linearization method[9] to system (2), the dynamics-based velocity controller for formation control is given by

$$\tau = \overline{B}_{-1}(-K_u\tilde{u}_2 + \overline{H}\dot{u}_{2d} + \overline{V}u_{2d}) \tag{11}$$

where $\tilde{u}_2 = u_2 - u_{2d}$ is the velocity tracking error of the follower robot, and $K_u = \mathrm{diag}(k_{u_1} \quad k_{u_2})$ is positve defined.

The controller (10) and (11) results in the actual closed system in the form of

$$\dot{\tilde{q}} = -K_q\tilde{q} + F\tilde{u}_2 \tag{12}$$

$$\dot{\tilde{u}}_2 = -\overline{H}^{-1}K_u\tilde{u}_2 - \overline{H}^{-1}\overline{V}u_2 \tag{13}$$

where $\tilde{q} = q_d - q$ is the formation tracking error, and the term $F\tilde{u}_2$ in (12) appears as the perturbation to the exponential stable system $\dot{\tilde{q}} = -K_q\tilde{q}$. If the velocity tracking error $\tilde{u}_2$ in (13) approaches to zero, the formation tracking error $\tilde{q}$ will converge to zero.

Let P be the symmetric positive definite solution of the following Lyapunov equation

$$K_q^{\mathrm{T}}P + PK_q = -Q \tag{14}$$

where Q is symmetric positive definite matrix. Let $\lambda_{min}(Q)$ denote the smallest eigenvalue of the matrix Q. The stability of the resulted closed-loop equations (12) and (13) can be proved using the Lyapunov theory, as shown in the following part of this section.

Consider the composite Lyapunov function candidate

$$V(t) = \frac{1}{2}\tilde{q}^{\mathrm{T}}P\tilde{q} + \frac{1}{2}\tilde{u}^{\mathrm{T}}\overline{H}\tilde{u} \tag{15}$$

Differentiating (15) with respect to time along the solutions of (12) and (13) using inequality (6) yields

$$\begin{aligned}\dot{V}(t) =& \frac{1}{2}(\dot{\tilde{q}}^{\mathrm{T}}P\tilde{q} + \tilde{q}^{\mathrm{T}}P\dot{\tilde{q}}) + \frac{1}{2}\tilde{u}_2^{\mathrm{T}}(\dot{\overline{H}} - 2\overline{V})\tilde{u}_2 - \tilde{u}_2^{\mathrm{T}}K_u\tilde{u}_2 \\ =& -\frac{1}{2}\tilde{q}^{\mathrm{T}}Q\tilde{q} + \tilde{q}^{\mathrm{T}}PF\tilde{u}_2 - \tilde{u}^{\mathrm{T}}K_u\tilde{u} \\ \le& -\frac{1}{2}\lambda_{min}(Q) \parallel \tilde{q} \parallel^2 + \\ & \lambda_{max}(P) \parallel F \parallel\parallel \tilde{q}^{\mathrm{T}} \parallel\parallel \tilde{u}_2 \parallel - \lambda_{min}(K_u)\|\tilde{u}_2\|^2\end{aligned} \tag{16}$$

where $\lambda_{max}(P)$ denotes the maximal eigenvalue of matrix P. From (16), we have $\dot{V}(t) < 0$ provided that

$$\lambda_{min}(Q)\lambda_{min}(K_u) > 0.5\lambda_{max}(P) \parallel F \parallel \tag{17}$$

and $(\tilde{q} \quad \tilde{u}_2) \neq 0$. Thus, the closed-loop systems (12) and (13) are stable when the condition (17) is satisfied.

The stability of the closed-loop system is guaranteed through the design of feedback gains in K_u and K_q, which satisfies the robustness inequality (17) by solving the Lyapunov equation (14).

Simulation results of the proposed formation control scheme are shown in Fig. 2. In Fig. 2(a), the leader robot first moves along a straight line, and then stops its straight line motion and rotates around itself. The follower robot tracks the lead with the desired relative distance and the desired relative bearing. As shown in Fig. 2 (b), both of the formation tracking errors converge to zero, and the steady value of the relative angular velocity is also zero, which indicates that the internal dynamics is stable.

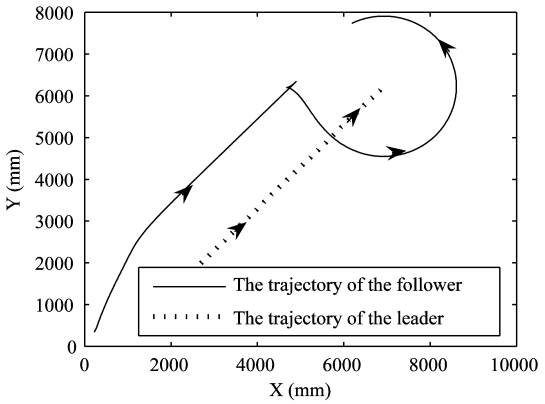

(a) The trajectories of two robots in formation

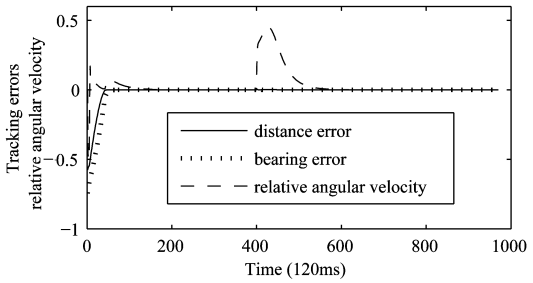

(b) The tracking errors and the relative angular velocity

Fig. 2 Simulation results using the proposed formation controller

When the condition (17) is satisfied, the perturbation $F\tilde{u}_2$ in (12) does not influence the stability of the formation kinematics system. Thus the influence of the velocity tracking error can be ignored, $\tilde{u}_2 = 0$, for the robot formation system. At this time, the kinematics-based system (9) can be treated as a independent system. Set $\bar{u}_{2d} = \widehat{u}_2$. The system (9) can be described by an equivalent kinematics model

$$\dot{q} = M_R(q \quad v_R \quad \omega_R) + F(q)\tilde{u}_{2d} \tag{18}$$

Although model (18) looks like the kinematics model given in [1∼3], they are quite different, since the motion

states in (18) are not the velocities of the leader robot relative to the environment as reported in [1∼3], but relative to the follower robot and measured from it. $\tilde{u}_{2d}$ is a desired velocity variation for the velocity $\hat{u}_2$. The equivalent kinematics model (18) will be used directly to derive the active obstacle avoidance controller in the next section.

3 Active obstacle avoidance

In this section, we will derive a novel obstacle avoidance algorithm for mobile robot based on the kinematics model of robot-obstacle system. Furthermore, an active obstacle avoidance controller will be obtained by integrating the algorithm into the formation system, and this controller will allow the follower to avoid obstacles within its field of view while following the leader with a desired relative bearing or distance.

3.1 Basic obstacle avoidance

The system of robot and obstacle is depicted in Fig. 3, where $\overrightarrow{\boldsymbol{v}}_2$ and $\overrightarrow{\boldsymbol{v}}_{obs}$ are the linear velocities of the robot and the obstacle, respectively. $\overrightarrow{\boldsymbol{v}}_{R_2} = \overrightarrow{\boldsymbol{v}}_2 - \overrightarrow{\boldsymbol{v}}_{obs}$ is the linear velocity that the robot is relative to the obstacle. The vector $\overrightarrow{\boldsymbol{v}}_{R_2}$ can be extended as a radial l_R. Clearly, if the accelerations of the obstacle and the robot are zero, and the radial l_R continually intersects with the obstacle, the collision between the robot and the obstacle will occur after the time $T_p = l_R / \parallel \overrightarrow{\boldsymbol{v}}_{R_2} \parallel$.

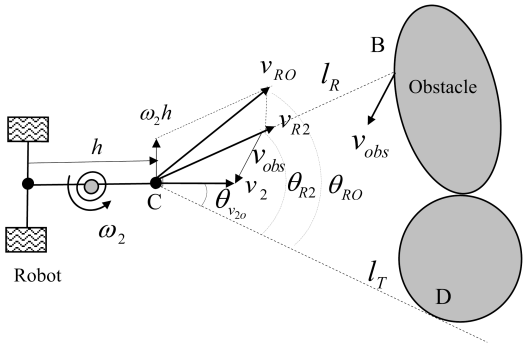

Fig. 3 The robot and obstacle system

To prevent the collision, the direction of $\boldsymbol{l}_R$ should be turned to point at the boundary (outer) of obstacle in the time T_p by adjusting the robot velocity. As shown in Fig. 3, define θ_{R_2} as angle from line $\boldsymbol{l}_R$ to the tangent $\boldsymbol{l}_T$, which is the tangent of the obstacle starting from the point C on the robot. Then, the target of avoiding the obstacle can be expressed as adjusting θ_{R_2} to zero within time T_p. Thus, the problem of obstacle avoidance is translated to control of θ_{R_2}.

The model of the follower robot and the obstacle system is given by

$$\dot{\theta}_{R_2} = \frac{v_{RO}\sin\theta_{RO}}{l_T} + [\frac{\sin\theta_{v_2O}}{l_T} \quad \frac{h\cos\theta_{v_2O}}{l_T}]\tilde{u}_{2d} \tag{19}$$

where $\overrightarrow{\boldsymbol{v}}_{RO} = \overrightarrow{\boldsymbol{v}}_2 + \omega_2 \overrightarrow{\boldsymbol{h}} - \overrightarrow{\boldsymbol{v}}_{obs}$ is the linear velocity that the follower robot is relative to the obstacle, and is observed from the view of the visual sensor fixed on the robot, such as a camera at point C. $\tilde{u}_{2d}$ is a desired velocity variation, as in the previous section, for the velocity $\hat{u}_2$. θ_{v_2O} is the angle between $\overrightarrow{\boldsymbol{v}}_2$ and $\boldsymbol{l}_T$. $\tilde{u}_{2d}$ is treated as control input to avoid the obstacle. To avoid collision with the obstacle, θ_{R_2} should satisfy the following condition

$$\dot{\theta}_{R_2} < -\frac{\theta_{R_2}}{T_p}$$

The condition (19) can also be expressed as

$$\dot{\theta}_{R_2} = -\alpha\frac{\theta_{R_2}}{T_p} \tag{20}$$

where $\alpha > 1$ is a positive constant. If condition (20) holds on, the robot will avoid the obstacle within a time less than T_p. A larger α leads to a rapider obstacle avoidance response. Substituting (20) into (19) and applying the feedback linearization method leads to the obstacle controller for the robot:

$$-\frac{\alpha}{T_p}\theta_{R_2} - \frac{v_{RO}\sin\theta_{RO}}{l_T} = [\frac{\sin\theta_{v_2O}}{l_T} \quad \frac{h\cos\theta_{v_2O}}{l_T}]\tilde{u}_{2d} \tag{21}$$

where α/T_p is the control gain.

3.2 Formation control with active obstacle avoidance

Both of the control inputs of (18) and (19) are the variations of $\hat{u}_2$ and based on the relative motion states. The comparability allows the part of the formation controller and the obstacle controller to be integrated together. The integration makes a motion coupling between the follower robot and the leader robot in the obstacle avoidance process. Then the follower robot can be guided by the leader robot to avoid the obstacle. Since the formation is partially kept when the follower robot is moving around an obstacle, as a result, the formation system will recover rapidly when the obstacle avoidance process is finished.

Recombine system (18) with (19), the partial formation system and the robot obstacle system are given by

$$\begin{pmatrix} \dot{\varphi}_{12} \\ \dot{\theta}_{R_2} \end{pmatrix} = \begin{pmatrix} v_R\sin\theta_{vR}/l_{12} - \omega_R \\ v_{RO}\sin\theta_{RO}/l_T \end{pmatrix} + F_{\varphi\theta}\tilde{u}_{2d} \tag{22}$$

$$\begin{pmatrix} \dot{l}_{12} \\ \dot{\theta}_{R_2} \end{pmatrix} = \begin{pmatrix} v_R\cos\theta_{vR}/l_{12} \\ v_{RO}\sin\theta_{RO}/l_T \end{pmatrix} + F_{l\theta}\tilde{u}_{2d} \tag{23}$$

where

$$F_{\varphi\theta} = \begin{pmatrix} -\sin\theta_{v2}/l_{12} & -h\cos\theta_{v2}/l_{12} \\ \sin\theta_{v_2O}/l_T & h\cos\theta_{v_2O}/l_T \end{pmatrix}$$

$$F_{l\theta} = \begin{pmatrix} -\cos\theta_{v2}/l_{12} & h\sin\theta_{v2}/l_{12} \\ \sin\theta_{v_2O}/l_T & h\cos\theta_{v_2O}/l_T \end{pmatrix}$$

The equations with respect to $\dot{\varphi}_{12}$ and $\dot{l}_{12}$ in (22) and (23) are used to describe the partial formation systems, respectively. Applying the feedback linearization method to the systems (22) and (23), respectively, we can obtain the active obstacle controllers, which are given by

$$F_{\varphi\theta}{}^{-1}\begin{pmatrix} -k_{q_2}\tilde{q}_2 - (v_R\sin\theta_{vR}/l_{12} - \omega_R) \\ -\frac{\alpha}{T_p}\theta_{R_2} - \frac{v_{RO}\sin\theta_{RO}}{l_T} \end{pmatrix} = \tilde{u}_{2d} \tag{24}$$

or

$$F_{l\theta}{}^{-1}\begin{pmatrix} -k_{q_1}\tilde{q}_1 - v_R\cos\theta_{vR}/l_{12} \\ -\frac{\alpha}{T_p}\theta_{R_2} - \frac{v_{RO}\sin\theta_{RO}}{l_T} \end{pmatrix} = \tilde{u}_{2d} \tag{25}$$

Remark. Using (24) or (25), the follower robot tries to keep partial formation with the leader during the obstacle

avoidance process. This means the follower robot is guided by the leader robot even when the obstacle occurs.

Two simulation results of the controller (24) and (25) are depicted in Fig. 4. In the simulation, the follower robot avoided the obstacle while keeping the desired relative bearing $\varphi_{12} = 2\pi/3$ as shown in Fig. 4(a), or a desired relative distance $l_{12} = 1.75$ m, as shown in Fig. 4(c), with the leader robot. As shown in Fig. 4(b) and Fig. 4(d), during the obstacle avoidance period, both the recorded maximum expected tracking error for the relative bearing and the relative distance along the time coordinate were bounded and did not exceed 0.1 (1.341%) and 26 mm (1.412%), respectively. We notice that the oscillations of the tracking errors in Fig. 4(b) and Fig. 4(d) were due to the high switching actions of the formation control and obstacle control. Furthermore, in the simulations the boundary of the obstacle is described by circles, so the direction of the tangent line from the robot to the obstacle boundary is continuously varying, and this is another reason for the oscillations.

Here we discuss the trigger condition for the active obstacle avoidance behaviour in formation control. When the follower keeps formation with the leader, if the control input $\tilde{u}_{2d}$ given by (10) satisfies the following condition

$$-\frac{\alpha}{T_p}\theta_{R_2} - \frac{v_{RO}\sin\theta_{RO}}{l_T} < [\frac{\sin\theta_{v_2O}}{l_T} \quad \frac{h\cos\theta_{v_2O}}{l_T}]\tilde{u}_{2d} \tag{26}$$

there the collision will not happen within time T_p , although the radial l_R intersects with the obstacle. The condition (26) means that the control input of formation keeping can also provide enough velocity variation input to avoid the obstacle. However, if (26) is not satisfied, the obstacle avoidance behavior should be triggered at the moment. Thus the triggered condition is synthesized as

$$\begin{cases} l_R \bigcap S \neq \Phi \\ -\frac{\alpha}{T_p}\theta_{R_2} - \frac{v_{RO}\sin\theta_{RO}}{l_T} > [\frac{\sin\theta_{v_2O}}{l_T} \quad \frac{h\cos\theta_{v_2O}}{l_T}]\tilde{u}_{2d} \end{cases} \tag{27}$$

where S is point set covered by the obstacle in Fig. 3, and Φ represents the empty set.

4 Experimental results

Experimental investigation has been conducted on a robot-soccer platform, which consists of three nonholonomic mobile robots and a visual measurement system, as shown in Fig. 5(a). The relative motion states used by formation controller are provided by a robot-fixed virtual sensor. The virtual sensor translates the information outputted by the measurement system into the relative position, relative orientation, and the relative motion states that are from the view of the follower robot.

A picture of three nonholonomic robots formation is shown in Fig. 5(b) where the leader robot R_1 in the robots

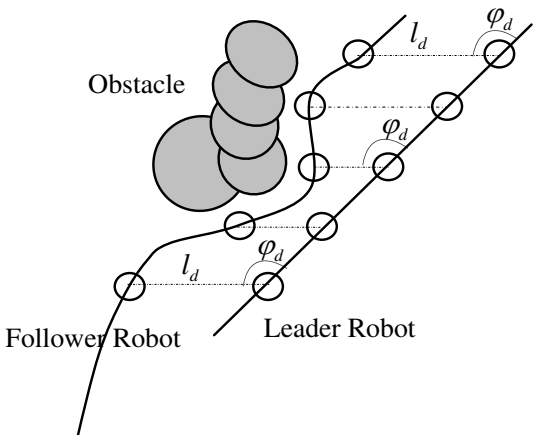

(a) The trajectories of the robots while the follower robot avoids the obstacle and tracks the leader robot with the desired relative bearing $\varphi_{12} = 2\pi/3$

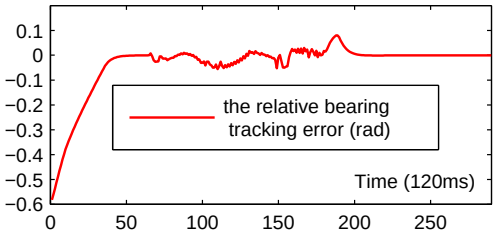

(b) The relative bearing tracking error

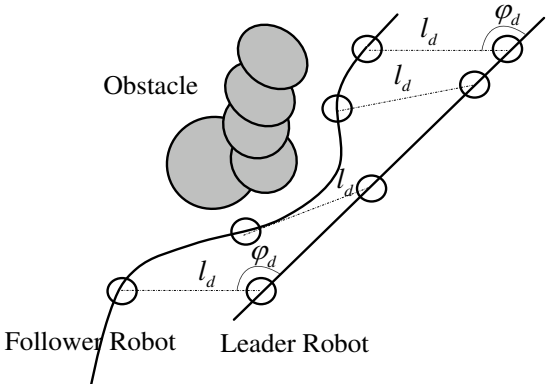

(c) The trajectories of the robots while the follower robot avoids the obstacle and tracks the leader robot with the desired relative distance $l_{12} = 1.75$m

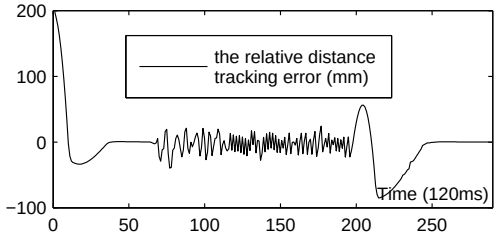

(d) The relative distance tracking error

Fig. 4 Simulation results using the proposed obstacle controllers

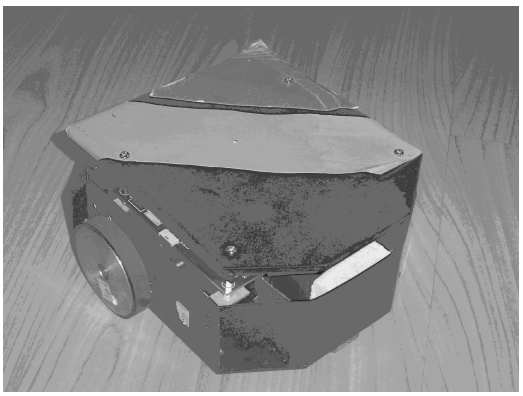

(a) The nonholomonic mobile robot used in the experiment

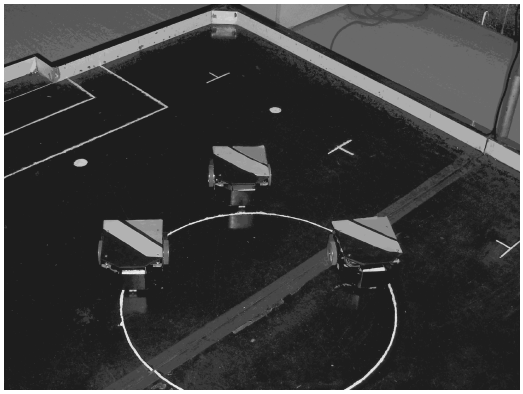

(b) Three robots formation moving

Fig. 5 The formation consisted of soccer robots

group is controlled by a joystick and runs an arbitrary trajectory, as shown in Fig. 6(a). Each follower robot in the robots group is controlled by a leader-follower controller with the desired separation $l_{12}^d = 40$cm and the desired relative bearing $\varphi_{12}^d = 2\pi/3$. To test the proposed formation controller in a more rigorous situation, the initial values for the relative orientation and the relative bearing are set to be $\varphi_{12} = 1.35\pi$ and $\phi_{12} = -0.6\pi$, respectively.

Under the proposed formation controller, the trajectories of the two robots, recorded by the vision system, are depicted in Fig. 6(a). The corresponding formation states are shown in Fig. 6(b) and Fig. 6(c). Both of the steady tracking errors are limited in 3.5%.

As shown in Fig. 6(d), the internal state ϕ_{12} keeps stable and varies around zero. Although severe oscillation appears in the internal state curve, but the oscillation has little impact on the formation tracking errors, as shown in Fig. 6(b) and Fig. 6(c). This shows the formation system is robust to the perturbation from the internal dynamics.

5 Conclusion

In this paper we have developed a formation control algorithm for mobile robots with active obstacle avoidance. The proposed method allows the follower robots to avoid obstacle while keeping the desired relative bearing or relative distance between robots. Furthermore, the controllers in this paper do not need the absolute velocity and position information from the global motion and localization sensory system, and this makes the proposed formation system easy to construct.

Acknowledgement

The authors are grateful to Zheng Wei and Wang Ting for instructions in experiments, and to Zhao Yi-Wen and Jing Xing-Jian for discussions during the early stages of the work.

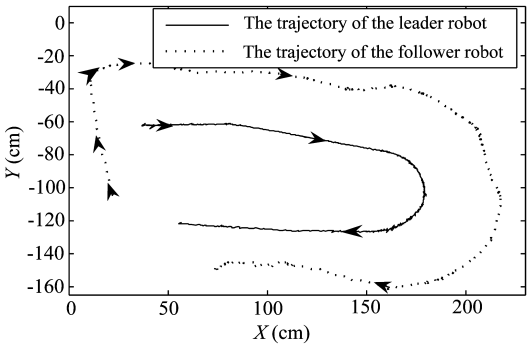

(a) The trajectories of the leader robot R_1 and the follower robot R_2

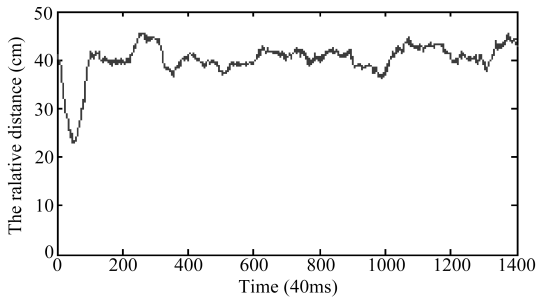

(b) The relative distance l_{12} between the leader robot R_1 and the follower robot R_2

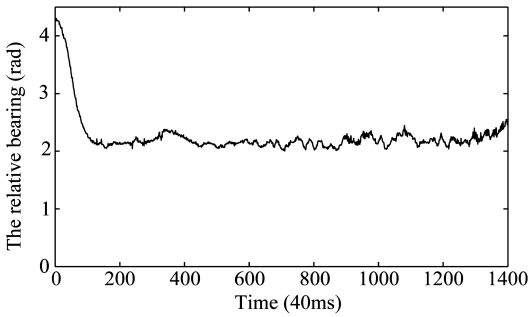

(c) The relative bearing φ_{12} between the leader robot R_1 and the follower robot R_2

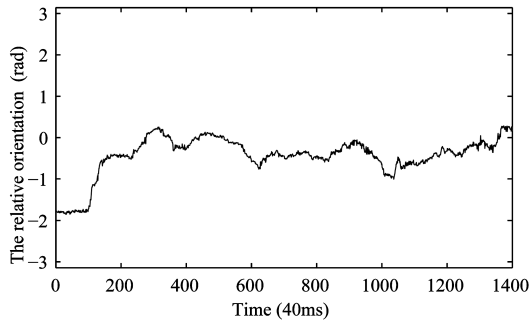

(d) The relative orientation ϕ_{12} between the leader robot R_1 and the follower robot R_2

Fig. 6 Experimental results

References

1 Das K, Fierro R, Kumar V, Ostrowski J P, Spletzer J, Taylor C J. A vision-based formation control framework. *IEEE Transactions on Robotics and Automation*, 2002, **18**(5): 813∼825

2 Desai J P, J Ostrowski, Kumar V. Modeling and control of formations of nonholonomic mobile robots. *IEEE Transactions on Robotics and Automation*, 2001, **17**(6): 905∼908

3 Desai J P, Ostrowski J, Kumar V. Controlling formations of multiple mobile robots. In: Proceedings of 1998 IEEE International Conference on Robotics and Automation. Leuven, Belgium, IEEE, 1998. **4**: 2864∼2869

4 Balch T, Arkin R C. Behavior-based formation control for multirobot teams. *IEEE Transactions on Robotics and Automation*, 1998, **14**(6): 926∼939

5 Fredslund J, Mataric M J. A general algorithm for robot formations using local sensing and minimal communication. *IEEE Transactions on Robotics and Automation*, 2002, **18**(5): 837∼846

6 Lawton J R T, Beard R W, Young B J. A decentralized approach to formation maneuvers. *IEEE Transactions on Robotics and Automation*, 2003, **19**(6): 933∼941

7 Clark C M, Frew E W, Jones H L, Rock S M. An integrated system for command and control of cooperative robotic systems. In: Proceedings of 11th International Conference on Advanced Robotics. Coimbra, Portugal, IEEE, 2003. 459∼464

8 Vidal R, Shakernia O, Sastry S. Distributed formation control with omnidirectional vision-based motion segmentation and visual servoing. *IEEE Robotics and Automation Magazine*, 2004, **11**(14): 14∼20

9 Slotine J J E , Li W. *Applied Nonlinear Control*. USA: Prentice Hall Incorporation, 1991. 207∼271

LIU Shi-Cai Received his bachelor degree from Wuhan University of Technology in 2001. He is a Ph. D. candidate at Shenyang Institute of Automation, Chineses Academy of Sciences. His research interest covers mobile robot modelling and control. Corresponding author of this paper.
E-mail: liushicai@sia.ac.cn

TAN Da-Long Received his bachelor degree from Tsinghua University in 1963. He is currently a professor of Shenyang Institute of Automation, Chinese Academy of Sciences. His research interest covers autonomous robots, applications of AI, and robotics to the industry and space probe.
E-mail: dltan@sia.cn

LIU Guang-Jun Received his bachelor degree from University of Science and Technology of China in 1984, master degree from Shenyang Institute of Automation, Chinese Academy of Sciences in 1987, and Ph. D. degree from University of Toronto in 1996, respectively. He is currently a tenured associate professor of Department of Aerospace Engineering, Ryerson University. His current research interest covers control systems, robotics, mechatronics, and aircraft systems.
E-mail: gjliu@ryerson.ca